Nanoscale Advances

ROYAL SOCIETY OF CHEMISTRY

PAPER

View Article Online
View Journal | View Issue

Cite this: *Nanoscale Adv.*, 2022, **4**, 1431

High-performance and selective adsorption of ZIF-8/MIL-100 hybrids towards organic pollutants†

Yukun Zhong,‡[a] Xueliang Mu‡*[a] and U Kei Cheang *[abc]

Environmental contamination by organic pollutants has become a pressing concern. In this study, metal–organic framework composites with a core–shell structure of MIL-100 wrapped around ZIF-8 (ZIF-MIL hybrids) were synthesized and characterized for their effectiveness to remove organic pollutants. First, a sequence of routine characterizations will examine the ZIF-MIL series samples' physicochemical properties and morphological characteristics. Then, the adsorption capacities of ZIF-MIL towards organic pollutants, including cationic dyes (methylene blue (MB), and rhodamine B (RHB)), anionic dyes (methyl orange (MO)), neutral pollutants (Sudan III (SD-III), tetracycline (TC) and amoxicillin (AMX)), were investigated. Among the ZIF-MIL series, ZIF-MIL-4 has an excellent specific surface area with high uptake of TC (1288 mg g^{-1}) and RHB (1181 mg g^{-1}). Based on the adsorption data from kinetic and dynamic studies, the adsorption process was closest to the pseudo-second-order kinetic model and Freundlich isotherm. In terms of thermodynamic parameter values, the adsorption of TC is an endothermic and spontaneous process, while the adsorption of RHB is an exothermic and spontaneous process. Furthermore, the reusability and selectivity studies of ZIF-MIL-4 towards TC and RHB exhibited significant regeneration ability and high selectivity. The effects of ionic strength and pH on pollutant removal efficiency were also tested. The experimental results showed that the main interactions between ZIF-MIL-4 and RHB or TC were weak coordination, electrostatic, hydrogen bonding, and π–π stacking interactions. Thus, the proposed MOF hybrid, by forming mixtures with other MOFs, can be a potential purifier with improved adsorption capacity and selectivity for organic pollutants as well as self-reusability.

Received 18th November 2021
Accepted 27th January 2022

DOI: 10.1039/d1na00819f

rsc.li/nanoscale-advances

1. Introduction

The pollution of water resources by organic pollutants has become a major concern in recent decades.[1] Among all sources of pollution, organic dyes and antibiotics in water systems are the most common organic pollutants in wastewater,[2] posing a serious potential threat to human health and the ecological environment. Although antibiotic concentrations in water are usually low, their low biodegradability can lead to adverse effects. For example, they can trigger the development of antibiotic resistance genes and chronic toxicity. Organic dyes completely resist the biodegradation process, interfere with photosynthesis and light transmission, are harmful to humans, and are carcinogens. Therefore, the removal of these contaminants from the environment is of utmost importance.

So far, organic pollutants are being removed using various methods, including adsorption,[3] membrane separation,[4] biodegradation, and photocatalytic oxidation.[5] Among them, adsorption is preferred because of its reasonable price, high efficiency, ease of use, and environmental friendliness.[6] However, most of the adsorbents available in the market share common disadvantages: low adsorption capacity, weak selectivity, and poor solid–liquid separation. Therefore, it is necessary to find an ideal adsorbent with high selectivity and adsorption capacity for organic pollutants.

Metal–organic frameworks (MOFs) are among the most popular crystalline porous materials and have significant advantages in diversity, porous structure, simple pore size and shape, high thermal and mechanical stability, large surface area, and ease of fabrication.[7] Due to their excellent water and thermal stability and numerous acid–base groups, ZIF-8 (zeolitic imidazolate framework-8) and MIL-100(Fe) are widely used for the adsorption separation of contaminants. MIL-100(Fe)[8] is a class of MOFs consisting of trivalent metal cations Fe^{3+} and carboxyl groups, and its two opening diameters are

[a]*Department of Mechanical and Energy Engineering, Southern University of Science and Technology, Shenzhen, 518055, China. E-mail: cheanguk@sustech.edu.cn; muxl@sustech.edu.cn; Tel: +86-755-88015352*

[b]*Shenzhen Key Laboratory of Biomimetic Robotics and Intelligent Systems, Southern University of Science and Technology, Shenzhen, 518055, China*

[c]*Guangdong Provincial Key Laboratory of Human-Augmentation and Rehabilitation Robotics in Universities, Southern University of Science and Technology, Shenzhen, 518055, China*

† Electronic supplementary information (ESI) available. See DOI: 10.1039/d1na00819f

‡ These two authors contributed equally to this work.

around 5.5 and 8.6 Å, respectively. In addition, ZIF-8 (zeolitic imidazolate framework-8)[9] is a zeolite SOD topology containing Zn^{2+} ions coordinated with imidazolium rings with pore diameters between 4 and 5 Å. Both of these MOFs have a large specific surface area and high performance. Moreover, their selectivity for target contaminants can be modulated by selective selection for metal ions and organic binders.[10]

Although removing hazardous substances from polluted aqueous environments by adsorption is one of the essential applications of MOFs, the adsorption capacity of MOFs is mainly unexplored. Due to the interfacial interactions between MOFs, the new structures generated by MOF@MOF may provide new opportunities for the development of MOF materials.[11] For example, one MOF@MOF adsorbent (Fe_3O_4@UiO-66@UiO-67/CTAB) was synthesized for Cr(VI) removal from solution with an excellent adsorption capacity of 932.1 mg g^{-1} (ref. 12) compared to the original MOFs (UiO-66 with 151.52 mg g^{-1} (ref. 13)). Although the performance of MOF@MOF is much better compared to the original MOFs, its specificity in the removal of organic contaminants has not been recognized. Therefore, it is necessary to explore the outstanding properties of MOF@MOF to find the ideal adsorbent material for selective adsorption of organic pollutants.

In this work, $Fe(SO_4)_2$ will be selected as the iron precursor using ZIF-8 as the supporter, and then the BTC precursor (Na_3BTC) will be prepared and deposited simultaneously on the surface of ZIF-8 (called ZIF-MIL hybrids) by a simple hydrothermal process. To evaluate the adsorption performance of thees ZIF-MIL hybrids on antibiotics and organic dyes, RHB (rhodamine B), MB (methylene blue), MO (methyl orange), AMX (amoxicillin), TC (tetracycline), and SD-III (sudan III) were chosen as representative impurities due to the fact that anionic and cationic dyes have the same toxicity, while TC and AMX belong to broad-spectrum antibiotics. The adsorption behaviors of RHB and TC were theoretically assessed using models. The effects of different factors (pH, ionic strength) in the removal process, the reusability and preferential uptake of RHB and TC from MO/RHB and MO/TC aqueous base respectively, and the uptake of TC and RHB from SD-III/TC and SD-III/RHB ethanol solution are evaluated and discussed.

2. Chemicals and methods

2.1. Chemicals

The chemicals used in this study are: 2-methylimidazole ($C_4H_6N_2$; CAS 693-98-1; Aladdin, China), trimesic acid (H_3BTC; CAS 554-95-0; Aladdin, China), zinc nitrate hexahydrate ($Zn(NO_3)_2\cdot 6H_2O$; CAS 10196-18-6; Aladdin, China), ferrous sulfate heptahydrate ($FeSO_4\cdot 7H_2O$; CAS 7782-63-0; Aladdin, China), sodium hydroxide (NaOH; CAS 1310-73-2; Aladdin), ethanol (EtOH, C_2H_5OH; CAS 64-17-5; Aladdin, China), methanol (MeOH, CH_3OH; CAS 67-56-1; Aladdin, China) and diethyl ether ($C_2H_5OC_2H_5$; CAS 60-29-7; Hushi, China). All chemicals were directly used as received without further purification. Deionized water used in experiments was purified from Milli-Q® Direct-Q 5. EtOH and MeOH were used as analytical reagents. RHB (CAS 81-88-9), MB (CAS 7220-79-3), MO (CAS 547-58-0), AMX (CAS 61336-70-7) were purchased from Aladdin. TC (CAS 60-54-8), and SD-III (CAS 85-86-9) were purchased from TCI Chemicals, China.

2.2. ZIF-8 fabrication

First, 3.25 g of 2-methylimidazole was dissolved in 50 mL of methanol with sonication. Then, 1.5 g of $Zn(NO_3)_2\cdot 6H_2O$ was dissolved in 20 mL of methanol and ultrasonic mixed in an ice water bath for 1 h and then transferred to a shaker with 200 rpm at 5 °C for over 8 h. The obtained white product was collected by centrifugation (5000 rpm, 3 min), washed with methanol five times. The above white product was soaked in methanol and placed in a suitable sized autoclave, sealed, and placed at 120 °C for more than 8 h. After the autoclave cooled down, the samples were removed and vacuum dried above 80 °C and ground into a white powder, stored at room temperature, and protected from moisture to complete the ZIF-8 preparation.

2.3. MIL-100 fabrication

First, 6 g of H_3BTC was added to an 8 mL aqueous solution containing 4 g of NaOH. The mixed solution was filtered to remove unreacted H_3BTC. An excess of ethanol was added to the filtrate to precipitate Na_3BTC. The resulting residue was washed repeatedly with ethanol ten times to remove unreacted NaOH and then washed with diethyl ether. Finally, the obtained white residue was placed in an evaporation dish and dried in an oven at 45 °C overnight to collect Na_3BTC powder.

Solution A included 0.93 g of Na_3BTC in 60 mL of DI water. Solution B consisted of 1.13 g $FeSO_4\cdot 7H_2O$ dissolved in 60 mL of water. The two solutions were mixed together for 15 h in the presence of air (shaking at 200 rpm in a shaker at 3 °C). The orange precipitate was separated from the supernatant by centrifugation and washed several times with deionized water and ethanol. The obtained solid was dried in a vacuum overnight and collected.

2.4. ZIF-MIL series samples fabrication

Separate solutions were prepared by dispersing ZIF-8 (0.23 g, 1 mmol) in a liquid mixture consisting of Na_3BTC (0.38 g, 1.4 mmol) and dissolving 0.46 g (3 mmol) of $FeSO_4\cdot 7H_2O$ in 25 mL of deionized water. The two solutions were mixed and then transferred to a constant temperature shaker to shake at 200 rpm for more than 8 h at a low temperature (2–8 °C). The resulting brownish-red precipitate was mixed at 5000 rpm for 3 min. The collected sample is washed five times with deionized water/methanol. The above reddish-brown precipitate was soaked in methanol and placed in a suitable sized autoclave, sealed, and placed at 120 °C for more than 8 hours. After the autoclave cooled down, the samples were removed and vacuum dried above 80 °C and ground into red-brown powder, and stored at room temperature, and protected from moisture to complete the ZIF-MIL series sample preparation. Syntheses with the same procedure, but keeping the molar concentration of ZIF-8 constant and varying the molar of $FeSO_4\cdot 7H_2O$ and Na_3BTC were performed. In this case: ZIF-MIL-1 (1 mmol of ZIF-8: 1.4 mmol of Na_3BTC: 3 mmol of $FeSO_4\cdot 7H_2O$), ZIF-MIL-2 (1 mmol of ZIF-8: 2.8 mmol of Na_3BTC: 6 mmol of $FeSO_4\cdot 7H_2O$), ZIF-MIL-4 (1 mmol of ZIF-8: 5.6 mmol of Na_3BTC: 12 mmol of $FeSO_4\cdot 7H_2O$), and ZIF-MIL-8 (1 mmol of ZIF-8: 11.2 mmol of Na_3BTC: 24 mmol of $FeSO_4\cdot 7H_2O$).

2.5. Apparatus

X-ray diffraction (XRD) analysis was performed in an X-ray diffractometer (Bruker D8 Advance) with a scan speed of 5° min^{-1} using Cu Kα radiation ($\lambda = 1.54$ Å) at a voltage of 40 kV and a scan range of 5–40° (2θ) with a step size of 0.02°. Fourier transform infrared (FTIR) analysis of the changes in the chemical functional groups of the ZIF-MIL mixture was performed using a Bio-Rad FTS 6000 spectrometer in the wavenumber range of 400 cm^{-1} to 2000 cm^{-1}. The morphology and crystal morphology of the ZIF-MIL series samples were studied in transmission electron microscopy (TEM, Thermo Fisher; FEI, F30). The atomic composition of the ZIF-MIL series samples was determined by energy dispersive spectroscopy (EDS, Oxford Instruments, INCA) to determine the elemental distribution. N_2 adsorption–desorption measurements were performed in a Micromeritics ASAP 2020 at −195.6 °C. The specific surface area of the samples was calculated using the multipoint Brunauer–Emmett–Teller (BET) equation in the range of P/P_0 of 0.05 to 0.99, while the total pore volume was determined at the saturation point of $P/P_0 = 0.997$. The ZIF-MIL series was vented at 200 °C for 6 hours before measuring the nitrogen uptake. To verify the thermal resistance of the samples, thermogravimetric analysis (TGA) was performed by Discovery TGA under N_2 atmosphere with a heat rate of 10 °C min^{-1}. X-ray photoelectron spectroscopy (XPS) analysis was collected on a PHI 5000 VersaProbe III (VAC PHI) with an aluminum monochromatic anode at an energy of 1486.6 eV. Survey spectra were collected in the energy range of 0–1400 eV.

2.6. Adsorption experiments

All batch adsorption tests were performed in the absence of light to prevent photodegradation of organic contaminants in aqueous solutions. Typically, a mixture of adsorbent and organic contaminants was placed in a constant temperature shaker and shaken at 200 rpm. The absorption performance of the different organic pollutants was tested by adding 1 mg of the ZIF-MIL series sample to an initial concentration of 100.0 mg L^{-1} of two cationic pollutants (RHB, MB), one anionic pollutant (MO), and three organic pollutants (AMX and TC in aqueous solution and SD-III in ethanol solution, respectively). Details of these six organic pollutants can be found in Table S1 (ESI).† The selective adsorption of the different contaminants was tested with 40 mL of the contaminant substrates RHB/MO, TC/MO, TC/SD-III, and RHB/SD-III using 200 mg of ZIF-MIL-4 mixture as adsorbent. The process was subsequently monitored by UV-vis spectroscopy.

Sampling was carried out at a predetermined time. Immediately after sampling, the sorbents were centrifuged. The absorbance at 251 nm (AMX), 357 nm (TC), 464 nm (MO), 556 nm (RHB), 666 nm (MB), and 507 nm (SD-III) was recorded using a UV-vis spectrophotometer, and a calibration curve was used to determine the residual concentration. The adsorption capacity of the contaminants was determined by eqn (1).

$$q_t = \frac{(C_i - C_t) \times V}{m} \quad (1)$$

where C_i and C_t (mg L^{-1}) represent the initial concentration and transient concentration of the solution respectively, V (L) and m (mg) are the volume of the contaminant solution and the mass of the adsorbent used respectively, and q_t (mg g^{-1}) is the transient adsorption capacity at adsorption time t (min).

Adsorption kinetics describes the adsorption rate of an adsorbent, which is determined by the contact time of the adsorption reaction. It is an important parameter in determining the adsorption efficiency and for interpreting the adsorption mechanism. In accordance with the equilibrium data, 20 °C was selected for the kinetic study. The adsorption equilibrium data of contaminants on ZIF-MIL samples were fitted with three well-accepted kinetic models, namely pseudo-first-order kinetics, pseudo-second-order kinetics, and intraparticle diffusion models, which are described below.

The pseudo first-order kinetics model is

$$\ln(q_e - q_t) = \ln q_e - k_1, \quad (2)$$

the pseudo-second-order kinetics model is

$$\frac{t}{q_t} = \frac{1}{k_2 {q_e}^2} + \frac{t}{q_e}, \quad (3)$$

and the intraparticle diffusion model is

$$q_t = k_p t^{0.5} + b, \quad (4)$$

where q_t (mg g^{-1}) is the transient adsorption capacity of pollutants on the ZIF-8/MIL-100 hybrids, q_e (mg g^{-1}) is the equilibrium adsorption capacity, k_1 and k_2 (min^{-1}) denote the constant of adsorption rate in eqn (1) and (2), and k_p (min^{-1}) represents the constant of diffusion rate for eqn (4), which is associated with the thickness of the boundary layer.

The adsorption isotherm describes the relationship between the equilibrium adsorption capacity of an adsorbent and the equilibrium concentration of a contaminant in a solution at a constant temperature. In isothermal adsorption experiments, a sample of 1 mg of ZIF-MIL was added to conical flasks containing 100 mL of aqueous solutions of TC and RHB at different concentrations (from 100 mg L^{-1}). The flask was shaken in a thermoregulatory shaker at 200 rpm for 8 hours thoroughly at 4, 20, and 36 °C. The experiments were performed in triplicate. For optimal modeling, laboratory equilibrium data were fitted to four isotherm models, *i.e.* Langmuir, Freundlich, Dubinin–Radushkevich (D–R), and Temkin isotherm models (see below).

Langmuir isotherm model,

$$\frac{1}{q_e} = \left[\frac{1}{q_m K_L}\right] \frac{1}{C_e} + \frac{1}{q_m} \quad (5)$$

where q_m (mg g^{-1}) and K_L (L mg^{-1}) are constants that are related to adsorption capacity and energy or net enthalpy of adsorption respectively, C_e is the concentration of pollutant solution at equilibrium (mg L^{-1}), q_e is the corresponding adsorption capacity (mg g^{-1}), and q_m (mg g^{-1}) and K_L (L mg^{-1}) are constants to measure adsorption capacity and energy or net enthalpy of adsorption respectively.

The Freundlich isotherm model is

$$\ln q_e = \ln K_F + \frac{1}{n}\ln C_e, \quad (6)$$

where K_F and n are the constants to estimate the adsorption capacity and intensity, respectively.

The D–R isotherm model is

$$\ln q_e = \ln q_s - K_{DR}\varepsilon^2, \quad (7)$$

where

$$\varepsilon = RT\ln\left(1 + \frac{1}{C_e}\right), \quad (8)$$

q_s (mg g^{-1}) is a constant of the D–R isotherm model that is correlated with adsorption capacity, K_{DR} (mol^2 kJ^{-2}) is a constant in relation to the mean free energy of adsorption E ($E = 1/\sqrt{2K_{DR}}$), T (K) is the absolute temperature, and R (8.314 J mol^{-1} K) is the gas constant.

The Temkin isotherm model is

$$q_e = K_T\ln f - K_T\ln C_e, \quad (9)$$

where K_T (L mg^{-1}) is the Temkin constant and f is the Temkin isotherm equilibrium binding constant.

The adsorption thermodynamics provide information about the inherent energy change of the adsorbent after adsorption and reveal the mechanisms of the adsorption. Free energy change (ΔG), enthalpy change (ΔH), and entropy change (ΔS) are calculated from adsorption isotherm data to determine the energy conversion of the adsorption process, as follows:

The enthalpy change is

$$\ln C_e = \frac{\Delta H}{RT} + c, \quad (10)$$

where c is integration constant,

the free energy change is

$$\Delta G = -nRT, \quad (11)$$

and the entropy change is

$$\Delta S = \frac{\Delta H - \Delta G}{T}. \quad (12)$$

The ideal adsorption selectivity of TC over MO on ZIF-MIL-4 was calculated according to the following expression:

$$S = \frac{q_{TC}/C_{TC}}{q_{MO}/C_{MO}} \quad (13)$$

where S is the pollutant selectivity, q_{TC} and q_{MO} (mg g^{-1}) are the equilibrium adsorption capacity of organic pollutants on adsorbents, and C_{TC} and C_{MO} (mg L^{-1}) correspond to the initial concentration of different pollutants in the mixed solution.

3. Result and discussion

3.1. Materials and characterization

In Fig. 1(A), the obvious peaks at $2\theta = 7.30$, 10.35, 12.70, 14.80, 16.40, and 18.00° correspond to planes (110), (200), (211), (220), (310), and (222), respectively, indicating the high crystallinity of the prepared ZIF-8.[14] Meanwhile, the strong peaks at $2\theta = 6.61$, 9.35, 10.97, 11.46 and 13.24° correspond to planes (200), (220), (311), (222), and (400) respectively, indicating the high crystallinity of the synthesized MIL-100.[15] As the concentration of the MIL-100 raised during the synthesis process, a broadened peak was observed in the XRD patterns of the ZIF-MIL-1 samples, indicating the formation of nanoscale crystals and amorphous structures. Some characteristic peaks of ZIF-8 at 7.30, 10.35, 25.7, and 35° were retained, while characteristic peaks of MIL-100 at 6.61, 11.46 and 13.24° appeared. Changing the molar ratio between ZIF-8 and MIL-100 could further increase the intensity of the MIL-100 peaks. Surprisingly, no characteristic peaks of ZIF-8 were detectable in ZIF-MIL-X (X = 2–8), which may be due to the conversion of ZIF-8 to amorphous ZIF-8 in the sample. It should be known that amorphous MOFs are characterized by the retention of the basic building blocks of MOF but lacks long-range crystallinity.[16] Therefore, the crystalline state of MIL-100 changed from short-range crystallinity to long-range crystallinity as the addition of ZIF-8 decreased, while the opposite was observed for ZIF-8 during the synthesis of the ZIF-MIL series.

As shown in Fig. 1(B), the absorption bands associated with the ZIF-8 structures was clearly observed in the FTIR spectrum of the ZIF-MIL sample. The sharp peak at 421 cm^{-1} is attributed to the Zn–N stretch, while the C–N stretch of imidazole-2-carbaldehyde develops at 1045 cm^{-1}. The ZIF-8 signal in ZIF-MIL was barely visible, probably because of the low abundance of the ZIF-8 nuclei. Despite the presence of characteristic ZIF-8 peaks, the intensity of the MIL peaks in the ZIF-MIL series increased with increasing MIL-100 content. In particular, the peaks at 483, 759, and 1380 cm^{-1} are attributed to Fe–O, ν(C–H), and –O–C–O– groups in benzene, and these peaks were significantly enhanced in spectra of ZIF-MIL-4 and ZIF-MIL-8.

The TEM images in Fig. 1(C)–(H) show that the synthesized ZIF-8 particles were submicron-sized crystals with the sharp boundary. The EDS diagram in Fig. 1(I) shows the core–shell structure of ZIF-MIL-4, where Zn and N atoms were found in the inner part of the particles and Fe and O atoms were found in the outer domain, *i.e.*, the composite with MOFs@MOFs structure can consist of a core of ZIF-8 (Zn and N are characteristic elements) surrounded by a shell of MIL-100 (Fe and O are characteristic elements). In contrast, the MIL-100 particles were irregularly shaped submicron particles. This result is consistent with the results obtained by XRD and FTIR. The core–shell structure of ZIF-MIL can be further synthesized by changing the molar ratio of ZIF-8 to MIL-100 precursors (Fe^{3+} and BTC^-), *i.e.*, the black core was surrounded by transparent gray material. It is easy to see that the inclusions on the ZIF-8 surface gradually changed from disordered to ordered states as the ZIF-8 content decreased, which is similar to the aforementioned XRD result. From the XRD and FTIR of ZIF-MIL-1, it can be seen that it retained some characteristic peaks of MIL-100, but the peak shape is not sharp due to the excess of disordered states. At very low levels of ZIF-8 (*i.e.*, ZIF-MIL-4 and ZIF-MIL-8), it is evident from the results of sharp XRD and FTIR peaks that the MIL-100 in ZIF-MIL-4 and ZIF-MIL-8 retained their original

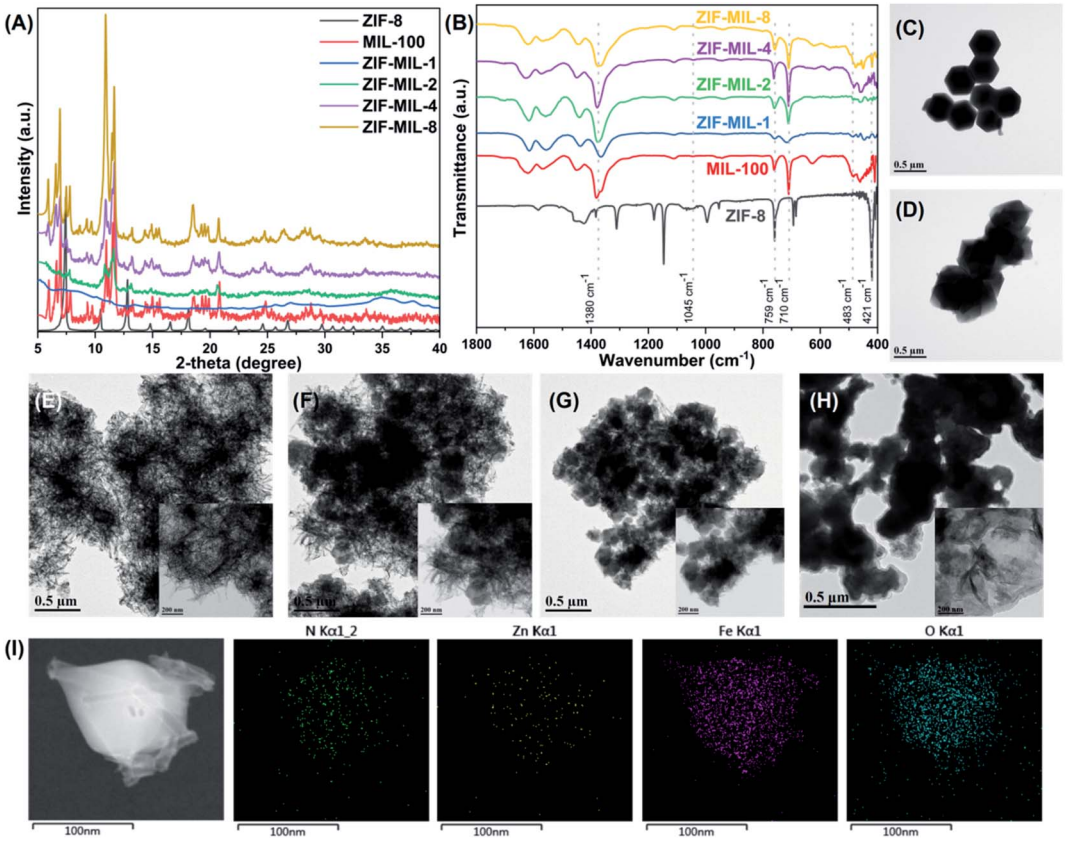

Fig. 1 (A) XRD patterns of ZIF-MIL series samples, (B) FTIR spectra of ZIF-MIL series samples, (C)–(H) the TEM images of ZIF-MIL series samples, (C) ZIF-8, (D) MIL-100, (E) ZIF-MIL-1, (F) ZIF-MIL-2, (G) ZIF-MIL-4, (H) ZIF-MIL-8, and (I) TEM image of ZIF-MIL-4 and corresponding mapping of four elements, N (green), Zn (yellow), Fe (purple), and O (blue), based on EDS.

characteristics after wrapping around ZIF-8. In spite of that, the TEM-EDS results from Table 1 demonstrate that the experimental molar ratio of MIL-100 to ZIF-8 is close to the theoretical value, which illustrates that the designed core–shell structure synthesis can produce effective hybrid structures with ZIF-8 core surrounded by MIL-100 shell.

The TGA tests confirmed the existence of ZIF-8 within the ZIF-MIL sample (Fig. 2(A)). A long plateau was observed in the temperature range of 150–500 °C, suggesting the high thermostability of ZIF-8 in its synthetic form. The first weight loss phase of ZIF-MIL started at about 350 °C due to the decomposition of MIL-100 in the hybrid. The ZIF-8 content of ZIF-MIL based on thermal stability and weight loss percentage is shown in Table 1. Theoretical weight loss percentages are very close to the experimental percentages except for ZIF-MIL-8. It is worth noting that the thermal resistance of ZIF-MIL-8 was slightly reduced, which may be due to the amorphous structure of ZIF-8 in the hybrid. Therefore, it is possible that the structural disruption of ZIF-8 occurred when a deficient amount of ZIF-8 encountered the MIL-100 precursor.

Nitrogen adsorption–desorption measurements of ZIF-8 and MIL-100 in Fig. 2(B) show type I isotherms. Isotherms of ZIF-8 and MIL-100 had a steep rise at low relative pressures (P/P_0 < 0.1), suggesting the presence of permanent micropores. Pore sizes of ZIF-8 and MIL-100, which were calculated using the Horvath Kawazoe (HK) method, were 10.024 and 10.894 nm. However, the ZIF-MIL series showed a type IV adsorption isotherm with a significant hysteresis, and the second absorption at high relative pressure indicates the presence of textured meso/macropores formed by nanoparticle packing. The pore diameters of the ZIF-MIL series were calculated using the HK method as 12.097, 12.309, 11.259, and 11.270 nm, respectively. Meanwhile, the presence of hysteresis indicated the deformation and swelling of ZIF-MIL. The difference in the adsorption properties of ZIF-MIL and ZIF-8 may be due to the influence of MIL-100. The presence of ZIF-8 and the amorphization caused by MIL-100 may affect their pore structures. The calculated specific surface areas (by BET and Langmuir) of ZIF-8 and MIL-100 were very similar to the previously reported values of ZIF-8 (ref. 17) and MIL-100 (ref. 18) samples prepared at room temperature, as shown in Table 1. When MIL-100 was added to the ZIF-MIL series, the specific surface area of the samples was decrease compared to ZIF-8, but in ZIF-MIL-4, the specific surface area was slightly higher than that of MIL-100. It was also found that the percentage of micropores increased with increasing MIL-100 content due to the reduced amorphization of MIL-100 and the lowered amount of amorphous ZIF-8 from the increased MIL-100 : ZIF-8 ratio.

ZIF-8 and MIL-100 have positive and negative surface charges, respectively, with zeta potential values of 32.48 and

Table 1 Physical features of ZIF-MIL series samples

	Sample	Fe[a] (wt%)	Zn[a] (wt%)	Molar ratio (MIL-100 : ZIF-8)	Theoretical molar ratio (MIL-100 : ZIF-8)
TEM-EDS	ZIF	0	17.73	0 : 1.00	0 : 1
	ZIF-MIL-1	23.97	14.13	1.51 : 1.00	1 : 1
	ZIF-MIL-2	24.75	3.83	2.50 : 1.00	2 : 1
	ZIF-MIL-4	23.26	2.26	3.98 : 1.00	4 : 1
	ZIF-MIL-8	26.02	1.30	7.74 : 1.00	8 : 1

	Sample	Theoretical ZIF-8 mass percentage	Experimental ZIF-8 mass percentage
TGA	ZIF-MIL-1	27.09%	28.69%
	ZIF-MIL-2	15.67%	12.49%
	ZIF-MIL-4	8.50%	8.70%
	ZIF-MIL-8	4.44%	9.99%

	Sample	BET specific area ($m^2\ g^{-1}$)	Langmuir specific area ($m^2\ g^{-1}$)	Micropore volume ($cm^3\ g^{-1}$)	Micropore percentage
Porosity	ZIF-8	1874.86	1977.89	0.67	93.51%
	MIL-100	1321.07	1615.60	0.45	72.03%
	ZIF-MIL-1	346.82	621.33	0.12	8.60%
	ZIF-MIL2	777.82	1363.28	0.28	22.32%
	ZIF-MIL-4	1336.40	1688.72	0.46	54.98%
	ZIF-MIL-8	923.22	1492.84	0.33	66.48%

[a] The wt% of Fe, Zn were obtained from EDS full spectrum scans of the elements (C, N, O, Fe, Zn).

−17.87 at pH = 7.0, as shown in Fig. 2(C). The surfaces of the ZIF-MIL series samples are more negatively charged as they were induced by the negative surface charge of the MIL-100 shell, which is consistent with the zeta potential of ZIF-MIL-*X* (*X* = 1–8). Contact of ZIF-8 or MIL-100 with water can raise or lower the pH, respectively, due to protonation of the exposed imidazole group (mim^-) in ZIF-8 or the binding of incompletely coordinated Fe^{3+} to hydroxide in the presence of water in MIL-100. In these cases, an increase in solution pH favors the interaction between the anionic contaminant and the positively charged ZIF-8 on the surface. Conversely, a decrease in the solution's pH favors the interaction between the cationic contaminant and the negatively charged surfaces of MIL-100. In addition, the partially coordinated Zn^{2+} in ZIF-8 and the benzene-tricarbonyl group in MIL-100 can, in turn, interact with hydroxides and protons in aqueous solutions, respectively. As stated, the whole series of ZIF-MIL adsorbents have negatively charged surfaces and also different adsorption sites, which should theoretically have significant adsorption effects on different types of organic pollutants. Thus, the ZIF-MIL obtained in this work can be used for the adsorption of various organic pollutants (anionic, cationic, and neutral).

3.2. Adsorption performance and mechanism

The results of the adsorption performance showed that one anionic pollutant (MO), two cationic pollutants (MB and RHB), and three neutral pollutants (TC, AMX, and SD-III) were effectively adsorbed by the ZIF-MIL samples with adsorption capacity ranging from 32 mg g^{-1} (SD-III, corresponding to 5 mg ZIF-MIL-1) to 658 mg g^{-1} (TC, corresponding to 5 mg ZIF-MIL-4), as shown in Fig. 3(A). ZIF-MIL-4 was found to be an effective adsorbent for the adsorption of contaminants in aqueous solutions (SD-III in ethanol solution). Fig. 3(B) shows the effect of adsorbent dose on the adsorption behavior of the six organic pollutants. The adsorption of each pollutant increased with decreasing dosage of ZIF-MIL-4. Among them, 1 mg ZIF-MIL-4 showed the highest adsorption for all organic pollutants with adsorption capacities of 1288 mg g^{-1} (TC), 534 mg g^{-1} (AMX), 399 mg g^{-1} (MO), 1181 mg g^{-1} (RHB), 404 mg g^{-1} (MB), and 254 mg g^{-1} (SD-III).

Electrostatic attraction is a major mechanism that affects the adsorption of organic pollutants by ZIF-MIL. There are two possible factors that influence adsorption capacity. One factor is the surface area, which can determine the differences in the adsorption performance of different adsorbents but does not ultimately determine the adsorption capacity of the adsorbent. The second factor contributing to the high adsorption capacity of contaminants is the electron donor–acceptor interactions on the MOF surface. Organic pollutants in the list usually contain π-electrons and readily interact with the π-electrons of ZIF-MIL *via* π–π-electron coupling. Notably, ZIF-MIL contains two sources of π-electrons, *i.e.*, imidazole and benzene rings. Their π–π stacking interactions with the π-electrons of organic pollutants further enhance the adsorption efficiency of organic pollutants. Thus, electrostatic attraction promotes the adsorption of organic pollutants.

In addition to electrostatic effects, there were other mechanisms for the adsorption of contaminants. Typical anionic

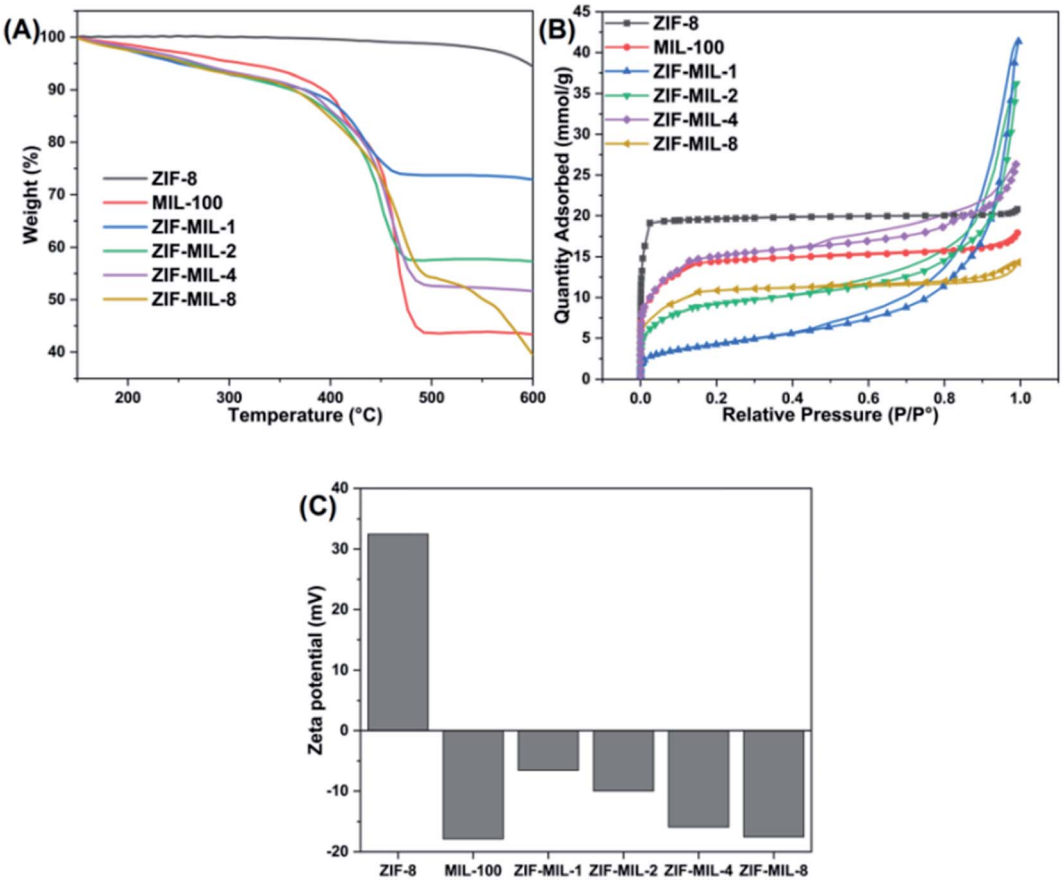

Fig. 2 (A) Thermal gravity analysis (TGA) of ZIF-MIL series samples, (B) N_2 adsorption–desorption isotherms of ZIF-MIL series samples, and (C) zeta potential of ZIF-MIL series samples (pH = 7).

contaminants, such as methyl orange (MO), were adsorbed mainly through electrostatic mechanisms. In aqueous solutions, the Fe^{3+} and Zn^{2+} open sites in MIL-100 and ZIF-8 were occupied by –OH,[19] but it was possible for OH to be substituted by other stronger Lewis bases.[20] For example, in the ZIF-MIL series, there may be an interaction between the $-SO_3^-$ of MO as a Lewis base[21] and the unoccupied Zn(II) and Fe(III) as Lewis acids, with the Lewis base $-SO_3^-$ of MO replacing –OH. In addition to a comparison between the zeta potential of pure ZIF-8 and pure MIL-100, ZIF-8 has more positively charged sites. That is, as a shell of MIL-100, it trapped MO molecules by capillary and internal pressure changes. The MO molecules

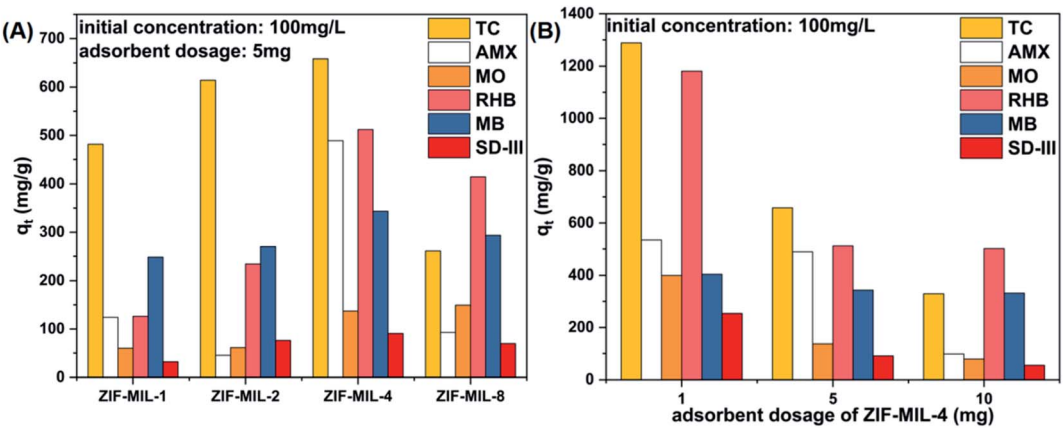

Fig. 3 (A) The adsorption performance ZIF-MIL samples towards 6 organic pollutants (the initial concentration being 100 mg L^{-1}, adsorbent dose being 5 mg, and solution volume being 100 mL). (B) The adsorption capacity of 6 organic pollutants with changing ZIF-MIL-4 dosages (the initial concentration being 100 mg L^{-1}, and solution volume being 100 mL).

were then pushed by repulsive forces from the negative surface of MIL-100 into the core of ZIF-8 and anchored in the ZIF-8 network. Meanwhile, the zeta potential decreases with increasing MIL-100 content, which corresponds to the increased adsorption capacity of MO in the ZIF-MIL series, *i.e.*, the immobilization of MO in the ZIF-MIL series was enhanced.

Based on the possible adsorption of anionic contaminants, the neutral SD-III adsorption of ZIF-MIL can be attributed to the –OH group in SD-III, which could cause the formation of hydrogen bonds with –NH/–COOH in ZIF-MIL. However, TC molecules are another neutral substance in an aqueous solution at pH 7 that can be adsorbed with a different adsorption mechanism. First, TC molecules are rich in hydroxyl, carbonyl, and π-electrons, which helps them to form H-bonds with ZIF-MIL through π–π interactions, *i.e.*, with $-NH_2$ and –COOH of ZIF-MIL. Second, unlike the two contaminants mentioned above, coordination can occur between Fe^{3+}/Zn^{2+} in ZIF-MIL and the electron-rich O-containing groups in acylamines (of TC). These two key factors synergistically contribute to the exceptionally high adsorption capacity of ZIF-MIL-4 for TC.

In addition to anionic and neutral organic pollutants, ZIF-MIL can be used to capture some cationic dye molecules (MB and RHB). The equilibrium adsorption capacity of ZIF-MIL-4 towards cationic dyes showed significantly better performance compared with other samples, as shown in Fig. 3. The adsorption capacity of ZIF-MIL-4 for RHB and MB may be due to the $-NH_2$/–COOH group and Zn^{2+}/Fe^{3+} in its structure. This promoted the formation of weak coordination interactions between the –COOH in RHB and the Fe^{3+} on the outer surface of ZIF-MIL-4 and the Zn^{2+} group inside, and the incompletely paired –COOH and $-NH_2$ groups also formed hydrogen bonds with the –COOH group in RHB. At the same time, the negatively charged surface of ZIF-MIL largely attracted the aggregation of the diethylamino end of RHB. In addition, the presence of the cation MB containing only dimethylamine ($-N(CH_3)_2$) can also lead to the formation of hydrogen bonds with ZIF-MIL, but the lack of weak coordination interactions makes the binding of MB to ZIF-MIL less effective.

3.3. Adsorption kinetics

To further investigate the adsorption process of TC and RHB, kinetic experiments were conducted. First, 1 mg of ZIF-MIL-4 was added to TC (100 mL, $C_0 = 100$ mg L^{-1}, pH = 7) or RHB (100 mL, $C_0 = 100$ mg L^{-1}, pH = 7) solutions. Fig. 4(A) shows the relationship between contact time and the amount of ZIF-MIL-4 adsorbed on TC and RHB. A rapid removal of TC and RHB was observed during the first 90 min, after which the adsorption process slowed down until equilibrium was reached. This phenomenon was due to the presence of many available adsorption sites and high concentrations of organic contaminants during the initial adsorption process; subsequently, the contaminant molecules were repelled, leading to a slow

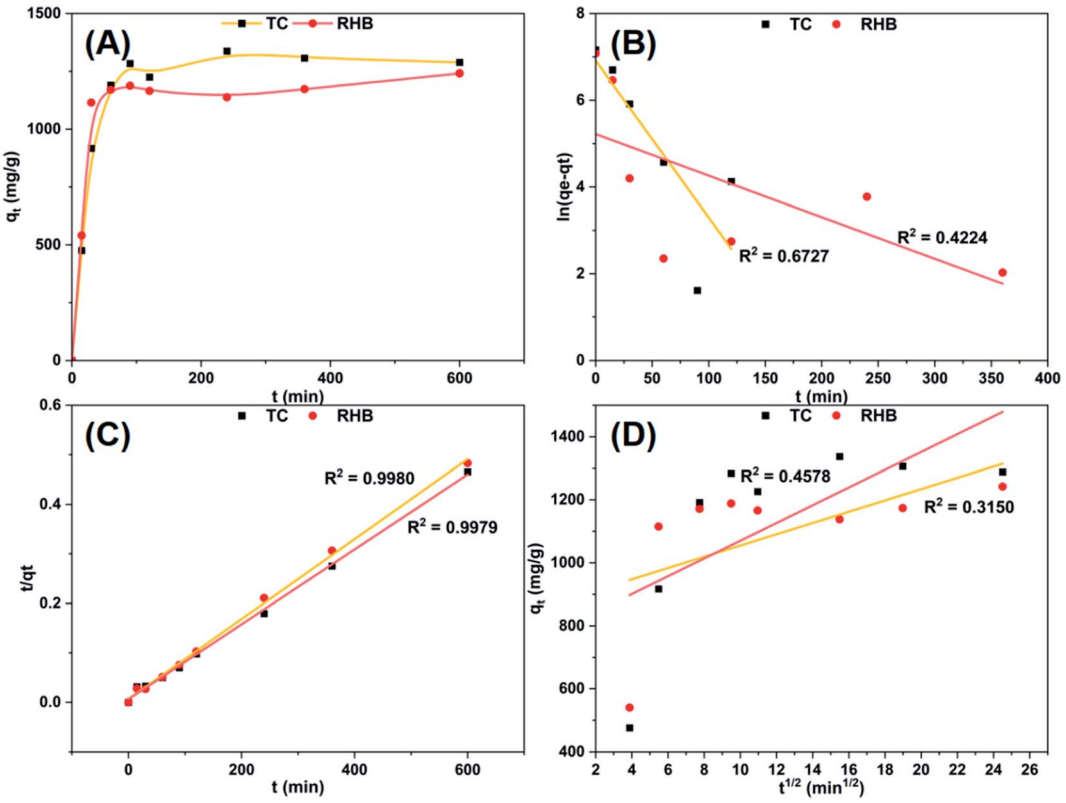

Fig. 4 (A) Adsorption equilibrium curves of RHB and TC on the ZIF-MIL-4. Adsorption equilibrium data process by (B) pseudo-first-order model, (C) pseudo-second-order kinetics model, and (D) intraparticle diffusion model (the initial concentration is 100 mg L^{-1}, the adsorbent dose is 1 mg, and the solution volume is 100 mL).

Table 2 Pseudo-second-order kinetic model parameters for the removal of RHB and TC on ZIF-MIL-4

		Pseudo-second order kinetic model		
Aqueous	$q_{e,exp}$ (mg g^{-1})	$q_{e,cal}$ (mg g^{-1})	k_2	R^2
RHB	1181	1184	1.96×10^{-6}	0.9980
TC	1288	1365	6.39×10^{-5}	0.9979

adsorption process that eventually reached the adsorption equilibrium. It should be noted that the equilibrium adsorption capacity of TC is higher than that of RHB. The increase in adsorption capacity may be due to the positive potential of the ZIF-8 core, which exerts a repulsive force on the positively charged RHB molecules. When the TC molecules were neutral in the pH range of 3.3–7.7,[22] there was no more any negative effect on the TC adsorption process of ZIF-MIL-4.

Fitting the adsorption equilibrium data of RHB and TC on ZIF-MIL-4 was performed according to three widely used models to explain the adsorption principle. Fig. 4(B)–(D) shows the relationship between the derived parameters based on adsorption time and adsorption capacity. It can be seen that the pseudo-second-order kinetic model gives a better fit with a higher correlation coefficient ($R^2 \approx 0.998$), and experimental equilibrium adsorption capacities agree well with calculated values in Table 2, indicating that chemisorption also occurred during the adsorption process. Two of the three octahedral Fe^{3+} ions of the compound MIL-100(Fe) have two terminal water ligands.[23] The octahedral environment of the third metal atom was realized by an anionic ligand (OH^-), which can be replaced by the electron-rich group (amine, carbonyl) of TC or attract cations (*e.g.* RHB). At the same time, additional adsorbed TC and RHB were transported to the ZIF-MIL-4 core (ZIF-8) through a concentration gradient. However, the charge potential of ZIF-8 was positive, and it had the same charge as RHB. The adsorption of contaminant molecules on the ZIF-MIL-4 core proceeded face-to-face, reducing the conjugation of π–π to RHB and maintaining the conjugation of π–π to TC until the equilibrium of adsorption and desorption was reached. Therefore, ZIF-MIL-4 was able to adsorb more TC than RHB.

3.4. Adsorption isotherm

The adsorption isotherms of two organic pollutants (RHB and TC) on ZIF-MIL-4 were determined at different temperatures (309.15, 293.15, and 277.15 K), as shown in Table 3. These results were performed using Freundlich, Langmuir, D–R, and Temkin isotherm models analysis. The corresponding equations of each isotherm model are given in the section on adsorption experiments. As seen from the isotherm parameters, the Freundlich model best described the data with coefficients of determination of 0.977–0.999 for RHB and 0.985–0.998 for TC. The Langmuir model also has a high coefficient of

Table 3 The parameters of the adsorption isotherms fitted by four models

		Model 1: Langmuir			Model 2: Freundlich		
Aqueous	T	q_m	K_L	R^2	K_F	n	R^2
RHB	309.15	8327	0.0013	0.9764	12.3756	1.0555	0.9766
	293.15	9027	0.0016	0.9914	18.7078	1.0918	0.9929
	277.15	9767	0.0018	0.9989	26.0912	1.1318	0.9985

		Model 3: D–R				Model 4: Termkin model		
Aqueous	T	q_s	β	E	R^2	f	K_T	R^2
RHB	309.15	1156	3.60×10^{-4}	37.2898	0.9066	0.0385	710.1833	0.9468
	293.15	1451	3.58×10^{-4}	37.3463	0.9451	0.0423	856.5165	0.9767
	277.15	1689	3.64×10^{-4}	37.0482	0.9851	0.0466	954.7409	0.9982

		Model 1: Langmuir			Model 2: Freundlich		
Aqueous	T	q_m	K_L	R^2	K_F	n	R^2
TC	309.15	6176	0.0035	0.9846	36.3536	1.2089	0.9891
	293.15	5876	0.0032	0.9804	30.6345	1.1902	0.9849
	277.15	4801	0.0024	0.9892	18.7077	1.1816	0.9977

		Model 3: D–R				Model 4: Termkin model		
Aqueous	T	q_s	β	E	R^2	f	K_T	R^2
TC	309.15	1765	2.60×10^{-4}	43.8616	0.9438	0.0505	978.2028	0.9768
	293.15	1589	3.02×10^{-4}	40.7183	0.9396	0.0489	891.5185	0.9713
	277.15	1063	3.96×10^{-4}	35.5523	0.9517	0.0443	606.2846	0.9824

determination for the linear correlation coefficient R^2. In contrast, their coefficients of determination for RHB are 0.976–0.999 and 0.980–0.989 for TC, indicating that the Langmuir model is less suitable than the Freundlich model. Thus, the Freundlich isotherm model suggests that the adsorption of TC and RHB on ZIF-MIL-4 was characterized by multilayer adsorption. Furthermore, TC adsorption exhibited higher adsorption capacity at higher temperatures, while RHB adsorption exhibited higher adsorption capacity at lower temperatures, indicating that the temperature had the opposite effect on the adsorption of these two pollutants. In addition, the q_e values increased with increasing C_e values. The results show that ZIF-MIL-4 was an effective adsorbent for the purification of TC and RHB in an aqueous solution.

3.5. Thermodynamic analysis

Since the description of the Freundlich model among the four models is most consistent with the adsorption isotherm, the Freundlich constant n was applied to determine the thermodynamic parameters. As shown in Table 4, $1/T$ exhibited good linearity with respect to n ($R^2 = 0.9999$ for RHB and $R^2 = 0.9432$ for TC). For RHB and TC, the negative ΔG values consequently reflect that the adsorption process was spontaneous. Both ΔH and ΔS of the adsorption process on TC have positive values, which proves that the adsorption process on ZIF-MIL-4 was endothermic and the adsorption reaction was favorable as the chaos degree and the temperature both increased. On the contrary, the ΔH and ΔS of the RHB adsorption process carry negative and positive values, respectively, which implies that the exothermic reaction will favor the adsorption process as the chaos and the temperature increase and decrease, respectively. Both are consistent with the adsorption isotherms results.

3.6. Effect of ionic type

The component of TC and RHB wastewater is usually quite complex, containing various ions, such as K^+, Na^+, Mg^{2+}, Ca^{2+}, Cl^-, NO_3^-, and SO_4^{2-}. The effect of ionic type (0.1 M) on TC and RHB removal was investigated in aqueous TC or RHB solutions. The existence of cations and anions had different effects on the adsorption efficiency of ZIF-MIL-4 on TC and RHB, as shown in Fig. 5(A). The presence of K^+, Na^+, NO_3^-, SO_4^{2-}, and Cl^- showed a positive effect on the process of TC removal, especially when K^+ was present in the aqueous solution, which increased its adsorption capacity by 1.7 times compared to the case with no extra ions. The presence of Ca^{2+} and Mg^{2+} had a significant negative effect on TC adsorption, probably because these two ions were able to complex with TC fractions and form flocs in water that cannot be adsorbed. Aqueous solutions of RHB and ZIF-MIL-4 showed completely different properties. The adsorption capacity of cations and anions (K^+, Na^+, and Cl^-) on ZIF-MIL-4 was increased at least 1.7-fold compared to the case with no additional ions. However, the presence of Ca^{2+}, Mg^{2+}, NO_3^-, and SO_4^{2-} decreased the adsorption capacity of ZIF-MIL-4 for RHB, where Ca^{2+} and Mg^{2+} may flocculated and agglomerated RHB molecules to the extent of preventing further adsorption, and where NO_3^- and SO_4^{2-} increased the solubility of contaminants in water. Therefore, the increased adsorption capacity of ZIF-MIL-4 on RHB and TC was mainly due to the presence of additional salts, the lower solubility of the contaminants in water, or the increased hydrophobicity between the pollutant molecules and the adsorbent, resulting in the increased removal of the contaminants. In the case of reduced RHB adsorption or increased TC adsorption, the addition of NO^{3-} or SO_4^{2-} would be a viable option to improve the selectivity of the pollutant.

The pH value can change the surface charge of the adsorbent and determine the degree of ionization of the contaminant in the solution, which in turn affected the adsorption capacity. In the acidic range, the dye is represented as a cation (RhB^+). As a result, electrostatic attraction occurred between RhB and the adsorbent, which led to an increase in adsorption capacity, as shown in Fig. 5(B). At higher pH values, RhB^+ was deprotonated and formed zwitterion. In addition, electrostatic repulsion may occur between RhB and the adsorbent, leading to a decrease in adsorption capacity in Fig. 5(B). TC molecules are amphiphile containing several ionizable functional groups. In the acidic range, TC species have TC^+ and TC^0 states, showing an increasing trend with increasing pH. The adsorption capacity for TC only increased when the pH increases to a slightly basic state (*i.e.*, around 9), as shown in Fig. 5(B). In this process, a strong electrostatic attraction between ZIF-MIL-4 and protonated TC or neutral TC was generated. A higher pH will lead to the deprotonation of TC and its negative charge will negatively affect the adsorption capacity of ZIF-MIL-4. Therefore, electrostatic effects played an important role in the entire physical adsorption process of ZIF-MIL-4 towards TC and RHB.

3.7. Reusability and selectivity

Based on the results of the adsorbent dosage shown in Fig. 3(B), the adsorbent dosage was further expanded in order to elucidate the relationship between the adsorbent dosage and the

Table 4 Thermodynamic parameters on the adsorption of RHB and TC in ZIF-MIL-4

Aqueous	T	n	R^2	ΔG (J mol^{-1})	ΔH (J mol^{-1})	ΔS (J mol^{-1})
RHB	309.15	1.0555	0.9999	−2712.99	−1759.46	2.8796
	293.15	1.0918		−2661.24		2.8603
	277.15	1.1318		−2607.94		2.8331
TC	309.15	1.2089	0.9432	−3107.35	1859.45	16.2350
	293.15	1.1902		−2900.97		16.4171
	277.15	1.1816		−2722.72		16.7217

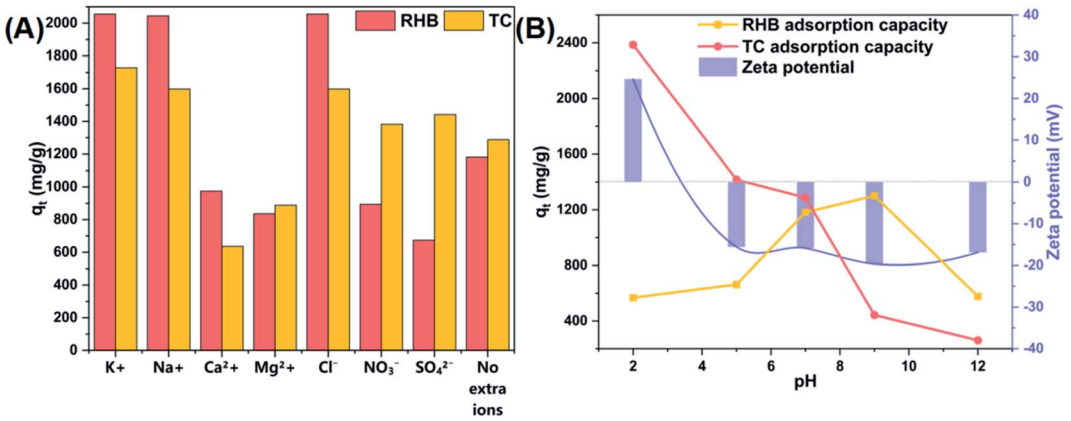

Fig. 5 Effect of (A) ionic type and (B) pH on the adsorption towards RHB or TC and zeta potential of ZIF-MIL-4.

adsorption efficiency of the adsorbent, as shown in Fig. 6(A). For the adsorption of two different pollutants, increasing the adsorbent dosage led to an increase in the adsorption efficiency. When the adsorbent dosage reached about 150 mg, the adsorption efficiency of both pollutants reached 95%. After that, the removal rate of RHB no longer varied with the increase of fresh adsorbent, while the removal rate of TC reached 100% when the adsorbent dosage reached 200 mg. Reusability of sorbents is important in practice, as reusability is directly related to cost savings. To evaluate the reusability of ZIF-MIL-4, the adsorption/desorption cycle of 200 mg of ZIF-MIL-4 was investigated. As for regeneration, the used material was washed five times with pure methanol and then soaked in 200 mL of methanol for 48 h at 80 °C. The samples were again activated

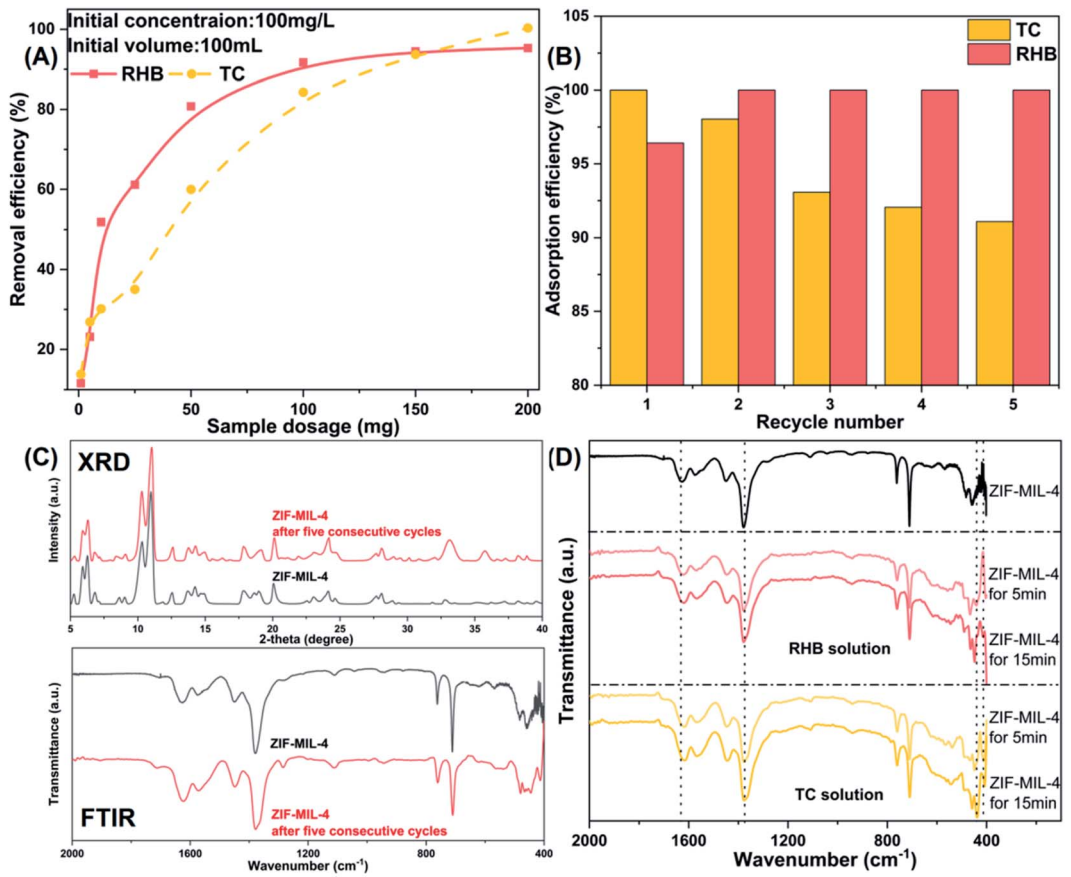

Fig. 6 (A) The extended sample dosage *versus* removal efficiency toward RHD and TC. (B) Recycling performance of reactivated ZIF-MIL-4 for five cycles. (C) FTIR analysis and XRD of ZIF-MIL-4 before and after five consecutive cycles. (D) FTIR analysis of ZIF-MIL-4 immersed in TC and RHD for 0 min, 5 min, and 15 min.

Table 5 Removal percentage of TC, RhB, and SD-III from their binary system using ZIF-MIL-4

		Mixed pollutant	Mixed portion			Removal rate (%)	
Dosage (mg)	V (mL)	A/B	mg (A)/mg (B)	Solution type	Selectivity	A	B
200	100	TC/MO	50/50	Water	3.94	90.18	30.12
		TC/RHB	50/50		1.16	98.79	90.29
		RHB/MO	50/50		3.87	86.87	26.35
		TC/SD-III	50/50	Ethanol	4.98	36.21	8.19
		RHB/SD-III	50/50		2.18	36.50	16.28

overnight in a vacuum oven at 100 °C before the next adsorption cycle. As shown in Fig. 6(a), the removal of virgin ZIF-MIL-4 by TC and RHB was 100% and 95%, respectively. After five consecutive cycles, the removal efficiency of TC and RHB were 91% and 100%, respectively, indicating a good cycling efficiency of ZIF-MIL-4. It is noteworthy that the basic porous structure of the samples was completely preserved after the adsorption/desorption cycle tests. Fig. 6(b) shows the XRD and FTIR of ZIF-MIL-4 after five consecutive cycles. The difference in the material structure before and after adsorption is negligible. The excellent reusability and structural stability suggest that ZIF-MIL-4 is a cost-effective and promising material for the adsorption of TC and RHB from wastewater in practical applications.

Separation of certain contaminants from a mixture of contaminants is more interesting and difficult. In this work, neutral TC (1.26 nm × 0.69 nm × 0.76 nm, 444.4 g mol^{-1}), cationic RHB (1.59 nm × 1.18 nm × 0.56 nm, 479.01 g mol^{-1}), anionic MO (1.31 nm × 0.55 nm × 0.18 nm, 327.33 g mol^{-1}), and neutral SD-III (1.57 nm × 0.73 nm × 0.68 nm, 352.4 g mol^{-1}) were chosen as models because of their different sizes, charges, and functional groups. ZIF-MIL-4 preferentially adsorbed neutral TC and positive RHB on TC/MO and RHB/MO substrates with selectivities of 3.94 and 3.87, respectively (see Table 5), due to electronic interactions (for all organic pollutants), coordination between Fe^{3+} of MIL-100 and acylamino groups (for TC), electrostatic between unliganded BTC^-/mim^- and diethylamine groups (for RHB), and π–π stacking interactions (for all organic pollutants). The selectivity of TC can also be increased up to 1.16 in aqueous solutions of TC/RHB mixtures, which may be due to the lower molecular weight and smaller molecular size of TC compared to RHB. The experiments also showed that the selectivity of TC isolated from TC/SD-III ethanol solution was 4.98, but the removal rate decreased to 36% because of the competition mechanism between the –OH (from ethanol) and the acylamino group (from TC) at the Fe^{3+} site. Thus, it can be inferred that ZIF-MIL-4 is a promising adsorbent for separating and concentrating certain organic contaminants from matrices, which will facilitate the corresponding subsequent analysis.

3.8 Insight of adsorption process

An in-depth understanding of the adsorption mechanism was investigated using FTIR. Fresh ZIF-MIL-4, two samples in RHB (ZIF-MIL-4 immersed in RHB solution for 5 min and 15 min), and two samples in TC (ZIF-MIL-4 immersed in TC solution for 5 min and 15 min) are shown in Fig. 6(D). Treated by two pollutant solutions, all four samples showed significantly enhanced variations in the following peak positions: 1570 cm^{-1}, 1360 cm^{-1}, 445 cm^{-1}, and 405 cm^{-1}, which correspond to COO^- stretch in zinc(II) carboxylates,[24] C–O stretch in iron(II) oxalate dihydrate,[25] the bending vibration of O–Fe–O bond,[26] and Zn–O stretching vibration,[27] respectively. This implies the presence of surface complexation between Fe(II) (or Fe(III))/Zn(II) in ZIF-MIL-4 and O-rich groups (including hydroxyl and carbonyl groups) in RHB and TC molecules, which is consistent with the chemisorption involved in the adsorption process.

Table 6 Comparison for the removal of TC and RHB by different adsorbents

Adsorbent	Organic pollutant type	q_m (mg g^{-1})	Ref.
MOF-525	TC	807	28
Y-GO-SA gel	TC	478	29
Fe-ZIF-8-500	TC	867	30
Co-doped UiO-66	TC	224.1	31
Ni doped FeO(OH)-NWs-AC	RHB	210	32
MIL-68(Al)	RHB	1111	33
Porous GO/hydrogel	RHB	769	34
ZnO/Zr-MOF(bpy)	RHB	919	35
ZIF-MIL-4	TC	1288	In this work
	RHB	1181	In this work

3.9 Comparison with other absorbents

Many previous studies investigated the removal of TC and RHB using different adsorbents. To evaluate the adsorption performance of ZIF-MIL-4 on TC and RHB, a list of the adsorption capacities from different adsorbents is presented in Table 6. These data show that the adsorption capacity of the synthetic adsorbent for both pollutants is significantly higher than most of the previously reported cases. In other words, ZIF-MIL-4 has excellent potential for rapid removal and efficiency under near-mild conditions. As a biocompatible and environmentally friendly material, ZIF-MIL-4 can be used in wastewater treatment for the removal of various environmental contaminants.

4. Conclusion

In summary, ZIF-MIL was successfully synthesized as a composite material with a core–shell structure using a simple

hydrothermal reaction process, as described above. The potential of these materials to remove organic pollutants from single and multi-component solutions was investigated using a design of experiments approach for different salt compositions, pH, temperature, and adsorbent dosage in solution. In our study, ZIF-MIL-4 showed a strong ability to adsorb TC (1288 mg g^{-1}) and RHB (1181 mg g^{-1}), especially in aqueous solutions alone, which performed better than other previously reported adsorbents in the removal of TC and RHB. According to the equilibrium studies, the uptake of TC and RHB in single pollutant solutions fits well with the Freundlich isotherm model, indicating a chemisorption process involving the removal of both pollutants by the ZIF-MIL-4 adsorbent. For binary aqueous solutions, the removal efficiency of TC and RHB remained very high, giving ZIF-8/MIL-100 a clear advantage for adsorbing the two types of pollutants over most of the existing adsorbents. When the pH and salt concentration change, lower pH and anions had diametrically opposing effects on TC and RHB adsorption. The two binary mixtures containing SD-III showed a much lower removal rate in alcohol solution, but the selectivity of TC was improved to 4.98. In a single solution, the kinetics of TC and RHB adsorption on the adsorbent follow a pseudo-second-order kinetic model. In addition, the adsorbent can be easily regenerated by immersion in methanol and high-temperature activation in a vacuum and reused in subsequent tests. Testing of the ZIF-MIL samples showed that the MOF-based hybrid material has the potential to be an efficient and practical adsorbent with high selectivity for the treatment of wastewater containing TCs and RHBs.

Author contributions

Ms. Yukun Zhong and Dr Xueliang Mu were mainly responsible for experimental design and operation, and wrote the whole article. Dr U Kei Cheang and Dr Xueliang Mu was responsible for providing suggestions on the experimental process and article revision.

Conflicts of interest

The authors declare that they have no conflict of interest.

Acknowledgements

This work was funded by the National Natural Science Foundation of China (NSFC, 51850410516), Department of Education of Guangdong Province (2021ZDZX2037), the Science, Technology, and Innovation Commission of Shenzhen Municipality (20200925155648005 and ZDSYS20200811143601004), the Shenzhen Municipal Government (Peacock Plan, 20181119590C) awarded to U Kei Cheang. The authors would like to acknowledge the SUSTech Core Research Facilities (SCRF) for technical support.

References

1 J. C. Sousa, A. R. Ribeiro, M. O. Barbosa, M. F. R. Pereira and A. M. Silva, *J. Hazard. Mater.*, 2018, **344**, 146–162.
2 J. K. Saha, R. Selladurai, M. V. Coumar, M. Dotaniya, S. Kundu and A. K. Patra, in *Soil Pollution-An Emerging Threat to Agriculture*, Springer, 2017, pp. 105–135.
3 A. M. Awad, R. Jalab, A. Benamor, M. S. Nasser, M. M. Ba-Abbad, M. El-Naas and A. W. Mohammad, *J. Mol. Liq.*, 2020, **301**, 112335.
4 H. Zhang, A. U. Mane, X. Yang, Z. Xia, E. F. Barry, J. Luo, Y. Wan, J. W. Elam and S. B. Darling, *Adv. Funct. Mater.*, 2020, **30**, 2002847.
5 P. Singh and A. Borthakur, *J. Cleaner Prod.*, 2018, **196**, 1669–1680.
6 D. S. Dlamini, J. M. Tesha, G. D. Vilakati, B. B. Mamba, A. K. Mishra, J. M. Thwala and J. Li, *J. Cleaner Prod.*, 2020, 123497.
7 X. Mu, Y. Chen, E. Lester and T. Wu, *Microporous Mesoporous Mater.*, 2018, **270**, 249–257.
8 M. Nehra, N. Dilbaghi, N. K. Singhal, A. A. Hassan, K.-H. Kim and S. Kumar, *Environ. Res.*, 2019, **169**, 229–236.
9 X. Mu, Z. Wang, Y. Zhong, T. Jiang and U. K. Cheang, *Ind. Eng. Chem. Res.*, 2021, **60**, 9465–9474.
10 S. Ramanayaka, M. Vithanage, A. Sarmah, T. An, K.-H. Kim and Y. S. Ok, *RSC Adv.*, 2019, **9**, 34359–34376.
11 S. Wu, G. Zhuang, J. Wei, Z. Zhuang and Y. Yu, *J. Mater. Chem. A*, 2018, **6**, 18234–18241.
12 L. Li, Y. Xu, D. Zhong and N. Zhong, *Colloids Surf., A*, 2020, **586**, 124255.
13 Y. Wang, N. Zhang, D. Chen, D. Ma, G. Liu, X. Zou, Y. Chen, R. Shu, Q. Song and W. Lv, *Sci. Total Environ.*, 2019, **682**, 118–127.
14 N. Ahmad, N. A. H. Md Nordin, J. Jaafar, N. A. N. Nik Malek, A. F. Ismail, M. N. F. Yahya, S. A. Mohd Hanim and M. S. Abdullah, *Particuology*, 2020, **49**, 24–32.
15 J. Koo, I.-C. Hwang, X. Yu, S. Saha, Y. Kim and K. Kim, *Chem. Sci.*, 2017, **8**, 6799–6803.
16 T. D. Bennett and A. K. Cheetham, *Acc. Chem. Res.*, 2014, **47**, 1555–1562.
17 E. Proietti, F. Jaouen, M. Lefèvre, N. Larouche, J. Tian, J. Herranz and J.-P. Dodelet, *Nat. Commun.*, 2011, **2**, 1–9.
18 L. W. Aguiar, G. P. Otto, V. L. Kupfer, S. L. Fávaro, C. T. P. Silva, M. P. Moisés, L. de Almeida, M. R. Guilherme, E. Radovanovic and E. M. Girotto, *Mater. Lett.*, 2020, **276**, 128127.
19 J. Kalmutzki Markus, N. Hanikel and M. Yaghi Omar, *Sci. Adv.*, 2018, **4**, eaat9180.
20 J. W. Yoon, Y. K. Seo, Y. K. Hwang, J. S. Chang, H. Leclerc, S. Wuttke, P. Bazin, A. Vimont, M. Daturi and E. Bloch, *Angew. Chem., Int. Ed.*, 2010, **49**, 5949–5952.
21 A. Charanpahari, S. S. Umare, S. P. Gokhale, V. Sudarsan, B. Sreedhar and R. Sasikala, *Appl. Catal., A*, 2012, **443–444**, 96–102.
22 Y. Zhao, X. Gu, S. Gao, J. Geng and X. Wang, *Geoderma*, 2012, **183**, 12–18.

23 Ü. Kökçam-Demir, A. Goldman, L. Esrafili, M. Gharib, A. Morsali, O. Weingart and C. Janiak, *Chem. Soc. Rev.*, 2020, **49**, 2751–2798.
24 V. Zeleňák, Z. Vargová and K. Györyová, *Spectrochim. Acta, Part A*, 2007, **66**, 262–272.
25 R. Rajagopalan and J. O. Iroh, *Electrochim. Acta*, 2001, **46**, 2443–2455.
26 S. R. Dhanya, S. G. Nair, J. Satapathy and N. Pavan Kumar, *AIP Conf. Proc.*, 2019, **2166**, 020017.
27 M. Matsumura, Z. Bandic and R. P. Camata, *MRS Online Proc. Libr.*, 2005, **869**, 17.
28 J. Xia, Y. Gao and G. Yu, *J. Colloid Interface Sci.*, 2021, **590**, 495–505.
29 J. He, F. Ni, A. Cui, X. Chen, S. Deng, F. Shen, C. Huang, G. Yang, C. Song, J. Zhang, D. Tian, L. Long, Y. Zhu and L. Luo, *Sci. Total Environ.*, 2020, **701**, 134363.
30 H. Yang, S. Hu, H. Zhao, X. Luo, Y. Liu, C. Deng, Y. Yu, T. Hu, S. Shan and Y. Zhi, *J. Hazard. Mater.*, 2021, **416**, 126046.
31 J. Cao, Z.-h. Yang, W.-p. Xiong, Y.-y. Zhou, Y.-r. Peng, X. Li, C.-y. Zhou, R. Xu and Y.-r. Zhang, *Chem. Eng. J.*, 2018, **353**, 126–137.
32 F. N. Azad, M. Ghaedi, A. Asfaram, A. Jamshidi, G. Hassani, A. Goudarzi, M. H. A. Azqhandi and A. Ghaedi, *RSC Adv.*, 2016, **6**, 19768–19779.
33 M. S. Tehrani and R. Zare-Dorabei, *RSC Adv.*, 2016, **6**, 27416–27425.
34 M. Shariati-Rad, M. Irandoust, S. Amri, M. Feyzi and F. Ja′fari, *Int. Nano Lett.*, 2014, **4**, 91–101.
35 W. Cui, X. Kang, X. Zhang and X. Cui, *J. Phys. Chem. Solids*, 2019, **134**, 165–175.